p-shell nuclei in a $(0+2)\hbar\omega$ model space. II. Results

A. A. Wolters, A. G. M. van Hees, and P. W. M. Glaudemans

Department of Physics and Astronomy, University of Utrecht, P.O. Box 80.000, 3508 TA Utrecht, The Netherlands

Several observables for the $A = 4-16$ p-shell nuclei, resulting from a calculation in the complete $(0+2)\hbar\omega$ model space, are presented. It is shown that the $2\hbar\omega$ admixtures are substantial. The calculated values of these observables are compared with the experimental data. Not only can the properties of many intruder states be reproduced correctly, but also the description of predominantly $0\hbar\omega$ states is often improved considerably.

I. INTRODUCTION

In a previous paper,[1] referred to as paper I, we presented an interaction for p-shell nuclei in the $(0+2)\hbar\omega$ model space. It was demonstrated that the mixing catastrophe could be avoided. As a result it was possible to describe both predominantly $0\hbar\omega$ states as well as intruder states, i.e., those states for which our calculation yields less than 50% $0\hbar\omega$ components. Furthermore, it was shown that the expansion of the model space gave rise to the presence of radially excited states, which in some cases can be identified experimentally.

The calculated spectra of the p-shell nuclei are compared with experimental data in Sec. II. The main structure of the $(0+2)\hbar\omega$ wave functions is presented in Sec. III. Section IV deals with charge radii, while static dipole and quadrupole moments are discussed in Sec. V. The main features of electromagnetic transition rates and $\log ft$ values are given in Secs. VI and VII, respectively. In Sec. VIII we discuss some problems related to the reproduction of electron-scattering form factors. Conclusions drawn from the present investigation are given in Sec. IX.

For a detailed discussion of the obtained results the reader is referred to Wolters.[2]

II. SPECTRA

The spectra, calculated with the interaction presented in paper I, and the measured ones are compared with each other in Figs. 1–26. Since we can only describe the normal-parity states in a $(0+2)\hbar\omega$ model space, the nonnormal-parity states are omitted from the experimental spectra. Because we used the binding energies of both ground states as well as excited states as input for the fitting procedure, these values are plotted. Only the Coulomb energy contribution has been removed from the experimental binding energies according to the procedure described in paper I. The experimental data have been taken from Fiarman[3] for ^{4}He and for $A = 5-16$ from Ajzenberg.[4-7] A discussion of the spectrum for each nucleus will be given below. Complete spectra and information on high-spin states can be found in Wolters.[2] For the intruder states we distinguish two classes: states of which the quantum numbers J^π and T can be formed also in a $0\hbar\omega$ model space (class-A states) and those of which the $J^\pi;T$ values cannot be formed in a $0\hbar\omega$ model space (class-B states).

A. Mass $A = 4$ nuclei

^4He: The excited states of ^{4}He are all unbound; see Fig. 1. The experimental information about energies and spins of normal-parity states with $T = 0$ in particular seems far from complete and often depends on a model-dependent analysis of phase-shift data.

Only two 0^+ states of ^{4}He have been included in the fit. In Fig. 1 one sees that both states are calculated at about the correct energy. In particular for the second 0^+ this is remarkable, because it is a well-known intruder state, which often is hard to reproduce correctly. Even if one removes this state from the fitting procedure, it is still calculated correctly with a deviation from the experimental energy of less than 0.5 MeV. Although the 0_2^+ state can be identified as a radial excitation, it lies barely above the breakup threshold. Its width of 0.05 MeV is small enough, so that it has been observed experimentally. The first 2^+ state seems to lie much too low in the present calculation. However, a lower-lying 2^+ state might have been observed experimentally at $E_x = 27$ MeV,[8,9] which would correspond much better with the present theoretical result.

There exist several shell-model calculations in which one attempts to describe the ground state and first excited 0^+ state in ^{4}He. We will restrict ourselves to a recent calculation,[10] because it has been performed in a very large model space. In this calculation the realistic two-body sussex interaction[11] was modified by multiplying the sussex matrix elements with an overall strength parameter. This parameter was determined by the condition that the calculated ground-state energy is fixed to the experimental value. The reported results for ^{4}He were obtained in a model space, which included all excitations up to $10\hbar\omega$. For the second 0^+ state the discrepancy between calculation and experiment decreased from 7 to 1 MeV, if the model space was enlarged from a $4\hbar\omega$ to a $10\hbar\omega$ space. This underlines the remarkable result of the present calculation, where one obtains similar energies in a much smaller model space.

B. Mass $A = 5$ nuclei

^5He: From Fig. 2 it follows that the broad $\frac{1}{2}^-$ state in ^{5}He with a width of about 1 MeV is correctly predicted, despite the fact that it was excluded from the fit. The calculated second $\frac{3}{2}^-$ and $\frac{1}{2}^-$ states, lying far above the breakup threshold, are identified as radial excitations of the first $\frac{3}{2}^-$ and $\frac{1}{2}^-$ states, respectively.

C. Mass $A = 6$ nuclei

^6Li: It follows from Fig. 3 that the lowest four levels of ^{6}Li are reproduced reasonably well. The theoretical 1_3^+, 2_2^+, and 3_2^+ states lie well above the breakup threshold. They are identified as radial excitations that belong to the $(\alpha+d)$ continuum. The 3_3^+ level calculated at $E_x=21$ MeV is not in agreement with the 3^+ assignment for the experimentally uncertain state at $E_x=15.8$ MeV. The yrast 4^+ state calculated at $E_x=20.2$ MeV may correspond with the observed $J^\pi=4^+$ state at $E_x \approx 23 \pm 2$

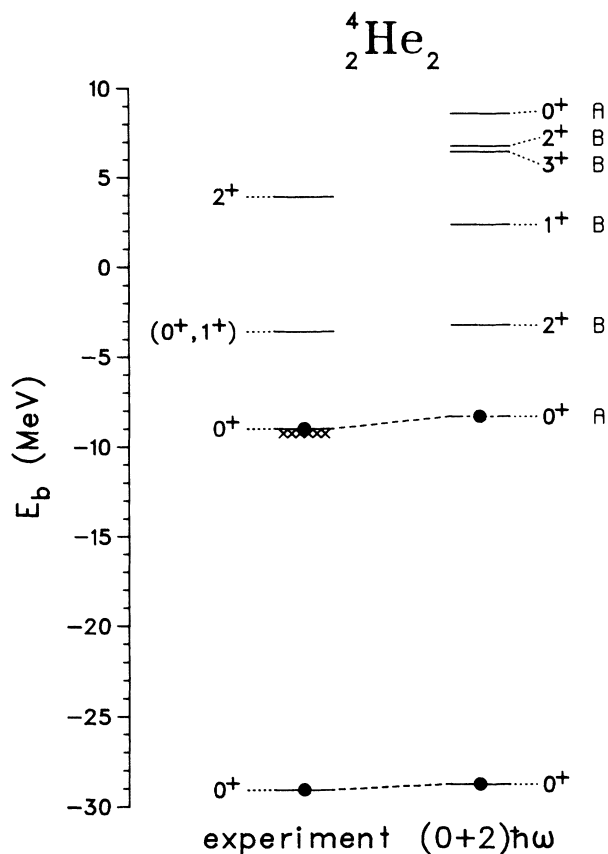FIG. 1. Spectrum of ^{4}He. Only normal-parity states with $T=T_z$ and at most four states with the same J are shown. Experimental and calculated states that are expected to correspond with each other, are connected by dashed lines. A solid dot indicates that the level is used as input in the fitting procedure. The class-A and class-B intruder states (see text) are labeled at the right-hand side. Levels identified as radially excited states (see text) are indicated by a chain-dotted line. The crosses show at which energy the nucleus becomes particle unstable.
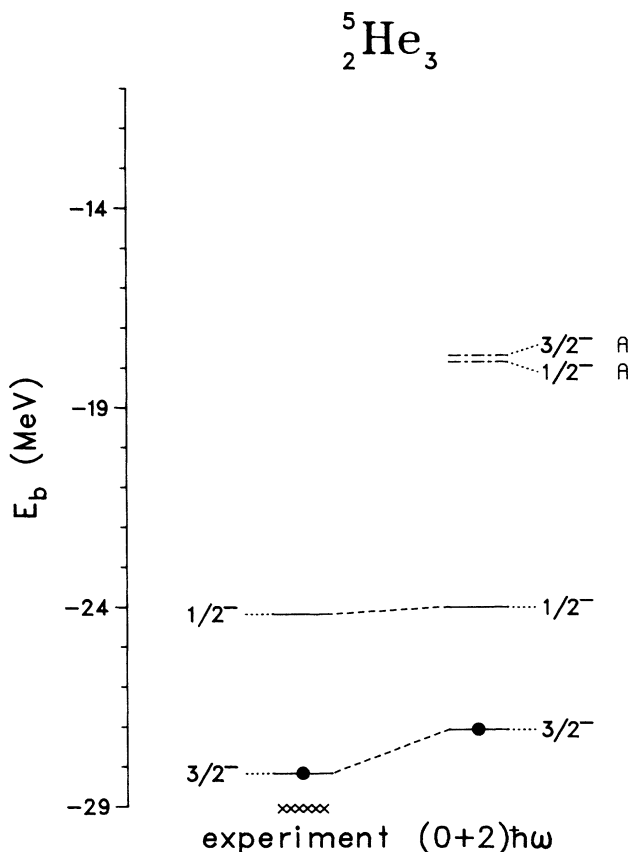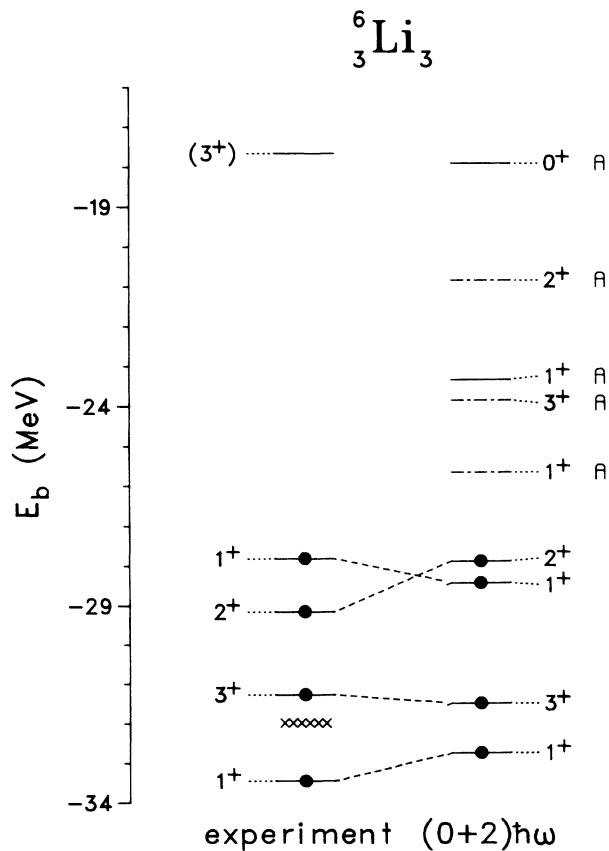

FIG. 2. Spectrum of ^{5}He. See also caption of Fig. 1.

FIG. 3. Spectrum of ^{6}Li. See also caption of Fig. 1.

MeV. The predicted lower-lying state with $J^\pi = 5^+$ at $E_x = 18.4$ MeV has not been observed so far.

^6He: The sequence of the lowest two states in ^{6}He is reproduced; see Fig. 4. There is no further experimental information available, however.

A calculation[12] in a $6\hbar\omega$ model space is reported for the $A = 6$ nuclei with a modified sussex interaction.[11] The results of that calculation for ^{6}Li are in good agreement with the experimental data. However, the presented spectrum[12] of ^{6}He contains several levels (a 0_2^+ state at $E_x = 6.5$ MeV, a 0_3^+ state at $E_x = 13.9$ MeV and a 2_2^+ state at $E_x = 23.3$ MeV), which are not reported in the experimental compilations. Some of the suggested extra levels, i.e., the 0_2^+ and 0_3^+ states, can also be found in the present calculation. They are not identified as radial excitations.

D. Mass $A = 7$ nuclei

^7Li: All five levels of ^{7}Li which were included in the fit are reproduced correctly; see Fig. 5. Also the calculated $\frac{3}{2}^-$ and $\frac{7}{2}^-$ states at $E_b = -31$ MeV agree with experiment as well as with the results obtained in a $0\hbar\omega$ model space.[13] The calculated $\frac{3}{2}_2^-$ and $\frac{1}{2}_2^-$ levels lying about 6 MeV above the breakup energy can be classified as radial excitations. The two states with the highest spin observed, $J^\pi = \frac{7}{2}^-$, are both well reproduced. Above $E_x = 10$ MeV the experimental information is scarce.

^7He: For ^{7}He only the binding energy of the ground

state is known experimentally. This value can be well reproduced in the present calculation; see Fig. 6.

E. Mass $A = 8$ nuclei

^8Be: From Fig. 7 one may conclude that the spectrum of ^{8}Be can be reproduced quite well, if one takes into account that the character of the 0_2^+ and 2_2^+ states can be explained by the phenomenon of radially excited states; see paper I. These levels can be considered as a discretization of the continuum. They have predominantly spatial symmetry $[f] = [44]$, i.e., can be identified as states containing two α clusters. Hence, one can find a theoretical counterpart for all experimental levels in the spectrum of ^{8}Be below $E_x \approx 20$ MeV. The experimental second 2^+ state belongs to an isospin-mixed doublet, and has therefore not been used in the fitting procedure. In $0\hbar\omega$ calculations[14,15] the 2_2^+ state has been obtained at a much too low excitation energy $E_x \approx 14.0$ MeV. However, it does not correspond with radial excitations. It is a state with almost pure spatial symmetry $[f] = [431]$. The $J^\pi = 4^+$ states have the highest spin observed and are well-reproduced theoretically.

^8Li: The lowest four levels of ^{8}Li, see Fig. 8, are calculated very accurately compared to older results. The two 2^+ states at $E_b \approx -38$ MeV are not observed experimentally. For the 0_1^+ and 1_3^+ states only one experimental level with a spin equal to 0 or 1 is available. The highest spin observed, i.e., $J^\pi = 4_1^+$, is predicted correctly.
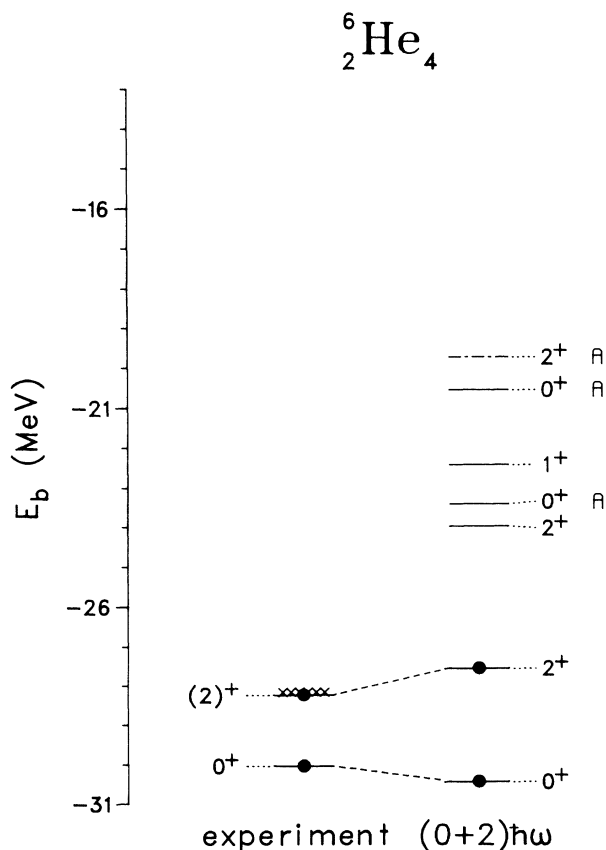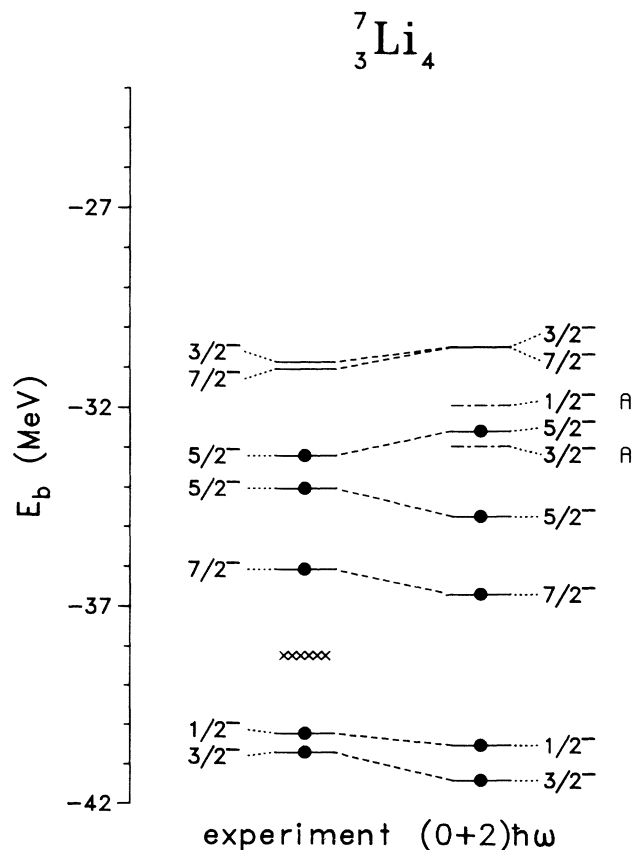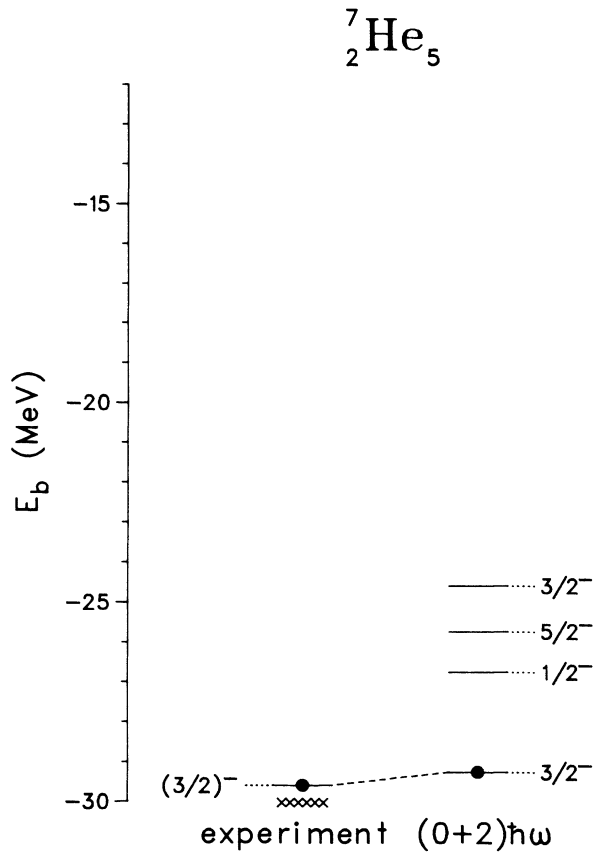

FIG. 4. Spectrum of ^{6}He. See also caption of Fig. 1.

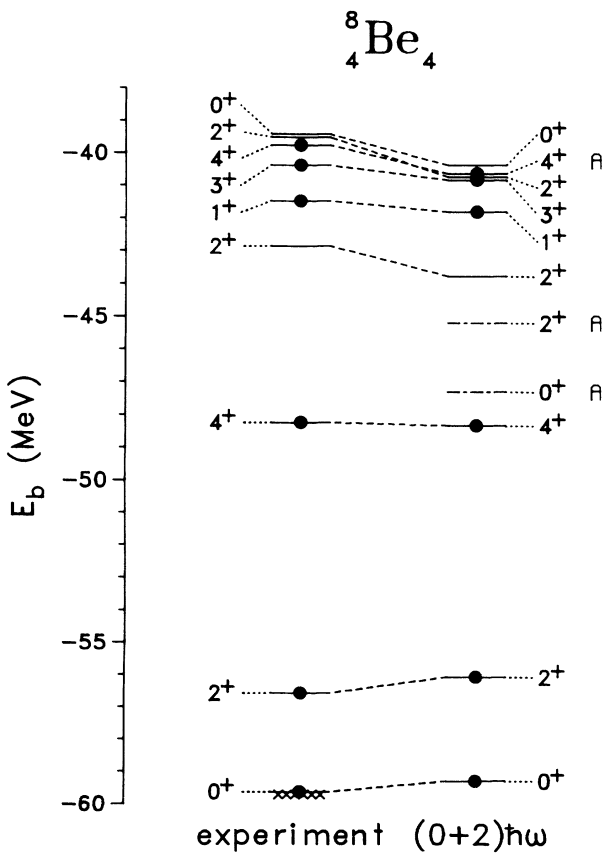FIG. 5. Spectrum of ^{7}Li. See also caption of Fig. 1.

$^{7}_{2}\text{He}_{5}$

FIG. 6. Spectrum of ^{7}He. See also caption of Fig. 1.

$^{8}_{4}\text{Be}_{4}$

FIG. 7. Spectrum of ^{8}Be. See also caption of Fig. 1.

^{8}He: The calculated binding energy of the ground state of ^{8}He, see Fig. 9, agrees well with the experiment. Except for the first excited state no more experimental data are available.

F. Mass $A = 9$ nuclei

^{9}Be: The four experimentally well known states of ^{9}Be are reproduced quite accurately; see Fig. 10. All other experimental data are unreliable. The second $\frac{3}{2}^{-}$ and $\frac{5}{2}^{-}$ states are also found in a $0\hbar\omega$ model space,[13] though there are no experimental candidates. The predicted $\frac{7}{2}_{2}^{-}$ state at $E_{x} = 10.9$ MeV might have been observed in the mirror nucleus ^{9}B at $E_{x} = 11.7$ MeV. The $\frac{3}{2}_{3}^{-}$ state about 10 MeV above the breakup threshold should be considered as a radial excitation of the ground state.

^{9}Li: The ground-state binding energy of ^{9}Li, see Fig. 11, as well as the suggested spin and parity $\frac{1}{2}^{-}$ for the first excited state are calculated correctly. The tentative assignment $J \geq \frac{9}{2}$ for the level at $E_{x} = 6.43$ MeV cannot be confirmed by the theory. All normal-parity states with $J \geq \frac{9}{2}$ are calculated at $E_{x} > 13$ MeV, while also no nonnormal-parity states with $J \geq \frac{9}{2}$ are expected below $E_{x} = 9$ MeV in the $1\hbar\omega$ model space.[13]

G. Mass $A = 10$ nuclei

^{10}B: In ^{10}B, see Fig. 12, the levels up to an excitation energy of 7 MeV are experimentally well investigated and

$^{8}_{3}\text{Li}_{5}$
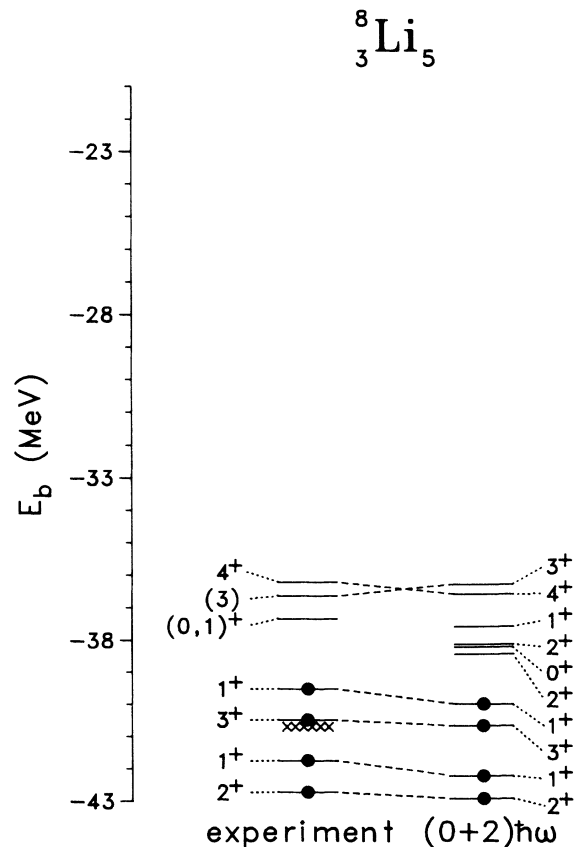
FIG. 8. Spectrum of ^{8}Li. See also caption of Fig. 1.

$^8_2$He$_6$
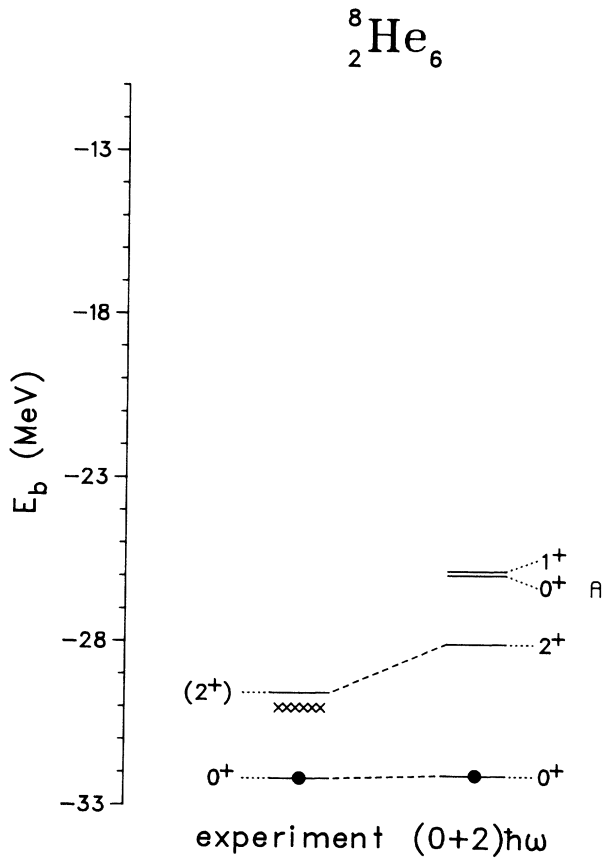
FIG. 9. Spectrum of ^{8}He. See also caption of Fig. 1.

$^9_3$Li$_6$
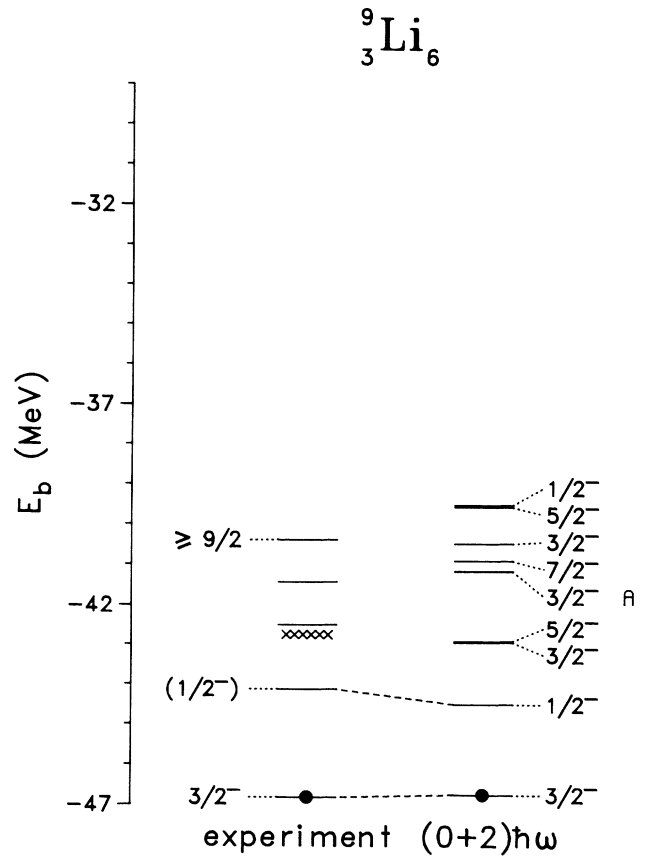
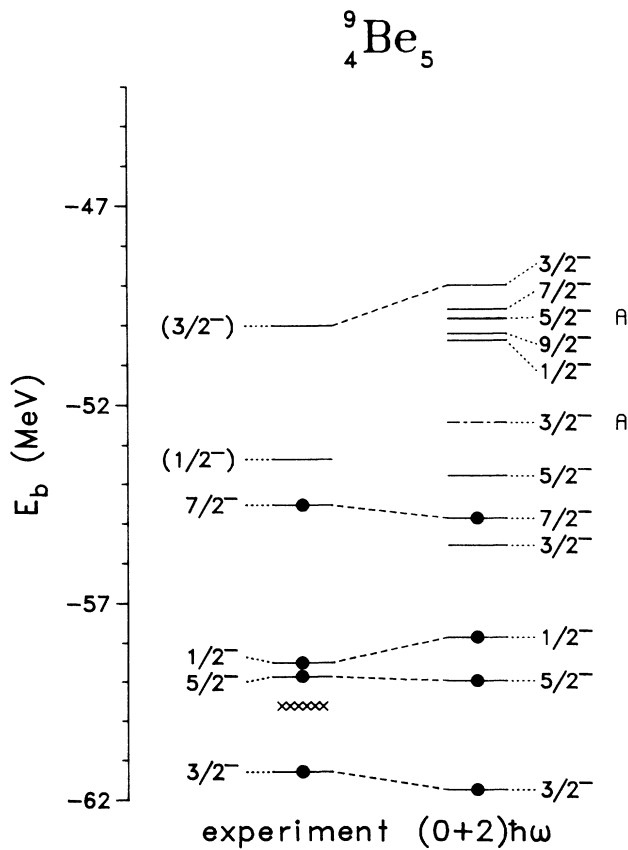FIG. 11. Spectrum of ^{9}Li. See also caption of Fig. 1.

$^9_4$Be$_5$

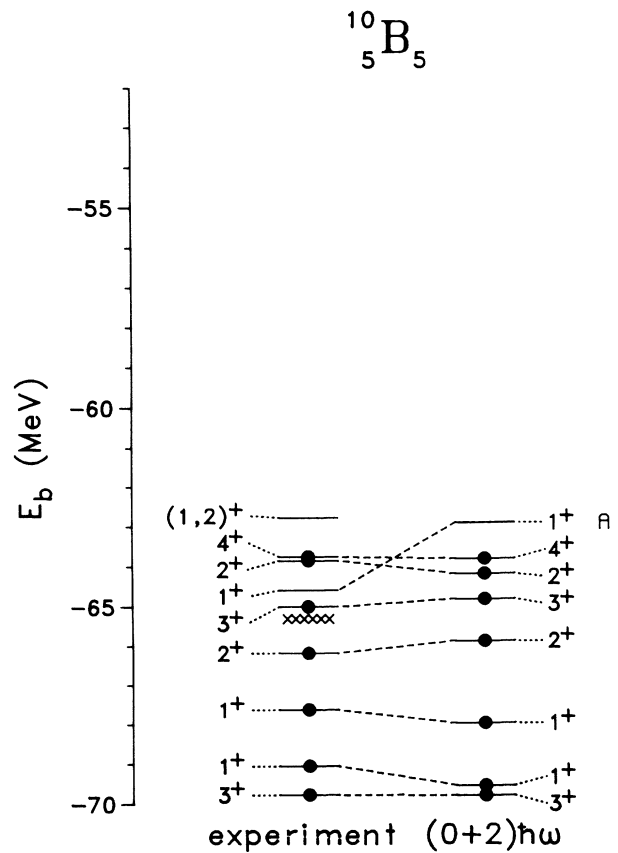FIG. 10. Spectrum of ^{9}Be. See also caption of Fig. 1.

$^{10}_5$B$_5$

FIG. 12. Spectrum of ^{10}B. See also caption of Fig. 1.

all theoretically reproduced. This data set includes the highest spin observed, $J^\pi = 4^+$. Above $E_x = 7$ MeV the experimental assignment of spin, parity, and/or isospin becomes uncertain, which prevents a comparison between calculation and experiment.

^{10}Be: If we restrict ourselves to normal-parity states, the experimentally known spectrum of ^{10}Be consists of 0^+ and 2^+ states only; see Fig. 13. The second 0^+ state at $E_b = -61.9$ MeV ($E_x = 6.2$ MeV) is an intruder state. This is evident, since in the $0\hbar\omega$ model space the excitation energy of the 0_2^+ state deviates about 12 MeV from the experimental value.[13] Presently it is calculated at $E_x = 7.4$ MeV, i.e., with a deviation of only 1.2 MeV.

H. Mass $A = 11$ nuclei

^{11}B: Fig. 14 shows that all levels of ^{11}B which were included in the fit, are calculated in the correct sequence. This holds also for the highest spin observed, $J^\pi = \frac{9}{2}^-$. Earlier $0\hbar\omega$ calculations[13] did not produce a theoretical candidate for the level with $J^\pi \le \frac{5}{2}^-$ at $E_b = -72.7$ MeV ($E_x = 8.5$ MeV). However, the present approach yields a candidate, the $\frac{3}{2}_3^-$ state. Taking into account the experimental spectrum of the mirror nucleus ^{11}C, one may assume that this level indeed should have $J^\pi = \frac{3}{2}^-$, since it is probably the analogue of the $\frac{3}{2}^-$ state in ^{11}C with $E_x = 8.1$ MeV. Similarly there exists a state in ^{11}C at $E_x = 10.0$ MeV with a tentative $\frac{7}{2}^-$ assignment. This would also agree well with the $\frac{7}{2}_2^-$ state calculated here.

^{11}Be: The experimental information of ^{11}Be is very scarce; see Fig. 15. The ground state has nonnormal parity, $J^\pi = \frac{1}{2}^+$, and can be well reproduced when $1\hbar\omega$ excitations are included in the model space.[13] Since the spin and parity of the observed second and third excited state are unknown, it is unclear to which of these the calculated $\frac{3}{2}^-$ and $\frac{5}{2}^-$ states should correspond.

I. Mass $A = 12$ nuclei

^{12}C: Several states of ^{12}C are found to be intruder states. It follows from Fig. 16 that the well known 0_2^+ intruder state is reproduced in beautiful agreement with experiment. The calculated 2_2^+ is a radial excitation. The experimental states with tentative assignments $J^\pi = 0_3^+$ and $J^\pi = 2_2^+$, respectively, at about $E_b = -89$ MeV are not found in the calculation. They may require the inclusion of $4\hbar\omega$ excitations in the model space.

^{12}B: Most of the normal-parity states in ^{12}B are reproduced; see Fig. 17. An exception might be the correspondence between experiment and theory for the 1^+ states. The second 1^+ state, calculated at an excitation energy $E_x = 3.75$ MeV, seems in rather poor agreement with the observed 1_2^+ in ^{12}B at $E_x = 5.00$ MeV. However, ^{12}N, the mirror nucleus of ^{12}B, shows a possible 1_2^+ state at $E_x = 3.56$ MeV, which has no known corresponding analogue in ^{12}B. Assuming that the calculated state corresponds with this level, the agreement between theory

FIG. 13. Spectrum of ^{10}Be. See also caption of Fig. 1.

FIG. 14. Spectrum of ^{11}B. See also caption of Fig. 1.

$^{11}_{4}Be_{7}$

FIG. 15. Spectrum of ^{11}Be. See also caption of Fig. 1.

$^{12}_{5}B_{7}$

FIG. 17. Spectrum of ^{12}B. See also caption of Fig. 1.

$^{12}_{6}C_{6}$

FIG. 16. Spectrum of ^{12}C. See also caption of Fig. 1.

$^{12}_{4}Be_{8}$

FIG. 18. Spectrum of ^{12}Be. See also caption of Fig. 1.

and experiment is very good.

^{12}Be: The nucleus ^{12}Be is one of the *p*-shell nuclei where none of the calculated low-lying states, shown in Fig. 18, has predominantly a 0ℏω configuration, i.e., all of these states have more than 50% 2ℏω components.

J. Mass *A* = 13 nuclei

^{13}C: The agreement between experiment and theory is considered good for ^{13}C; see Fig. 19. Not only the sequence of the lowest five levels is calculated correctly, but also several predictions correspond to experimental counterparts. All states shown above $E_b = -97$ MeV are class-*A* intruder states except the $\frac{1}{2}\frac{-}{3}$ state. The highest spin may have been observed for a state at $E_x = 13.4$ MeV with a tentative assignment $J^{\pi} = \frac{9}{2}^-$. This should be compared with the calculated value of $E_x = 15.6$ MeV for the $\frac{9}{2}^-$ yrast state (not shown).

^{13}B: Experimentally only the ground-state spin of ^{13}B is known. It follows from Fig. 20 that its binding energy is well reproduced. No spin values have been measured for any of the excited states, however. The relatively large gap calculated between the ground state and the excited states agrees with the present data. None of the calculated states shown has a predominant 0ℏω nature.

K. Mass *A* = 14 nuclei

^{14}N: In ^{14}N only the 1_1^+, 1_2^+, and 2_1^+ states have predominantly a 0ℏω nature, see Fig. 21. They are well
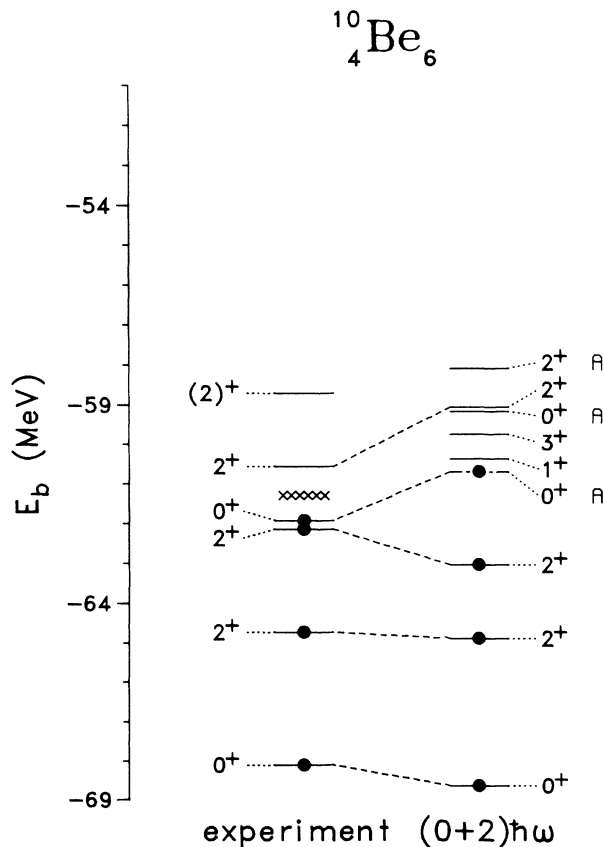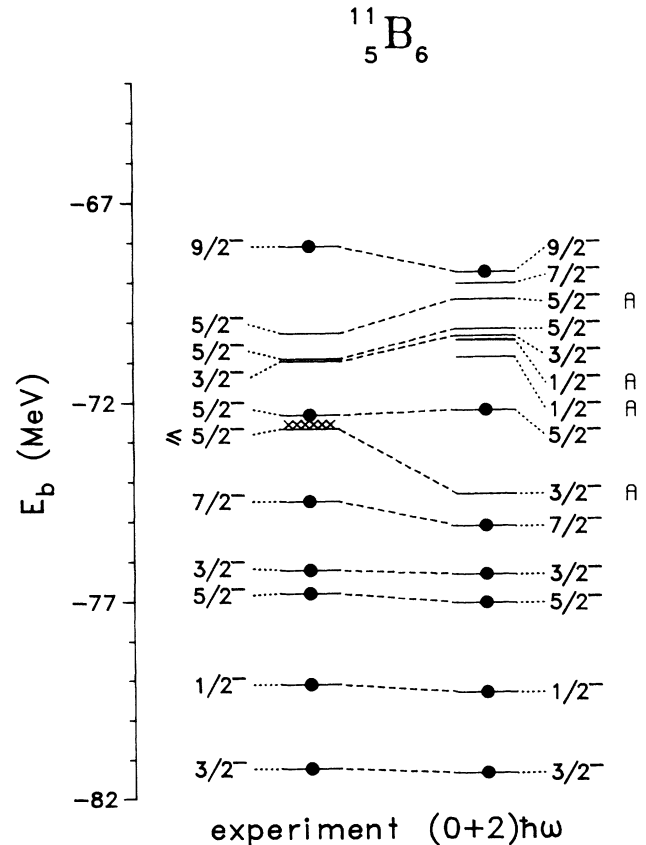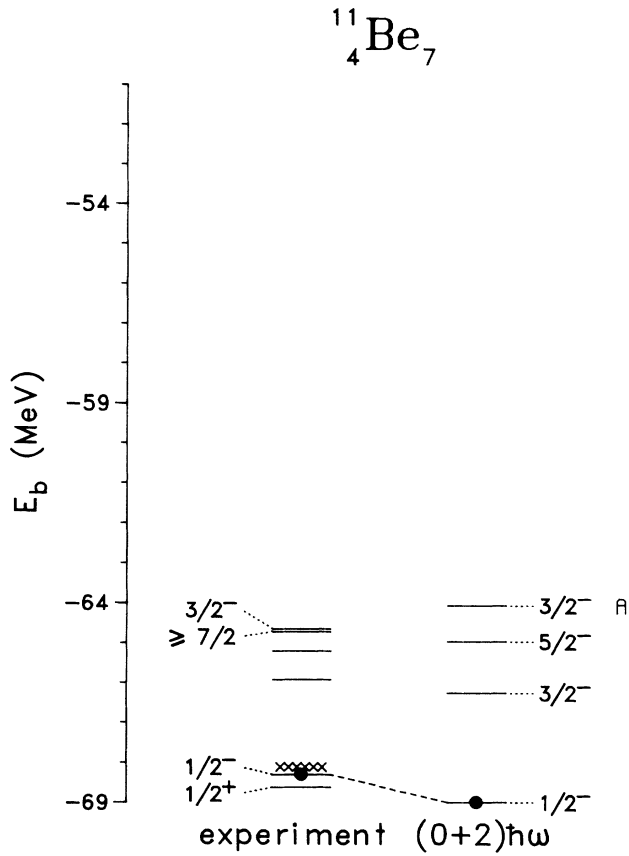

FIG. 20. Spectrum of ^{13}B. See also caption of Fig. 1.

FIG. 19. Spectrum of ^{13}C. See also caption of Fig. 1.

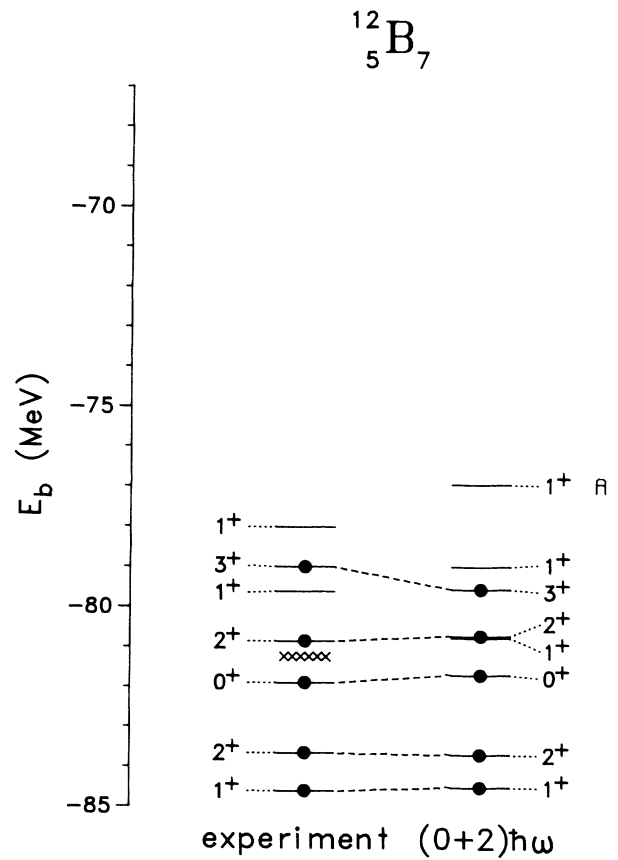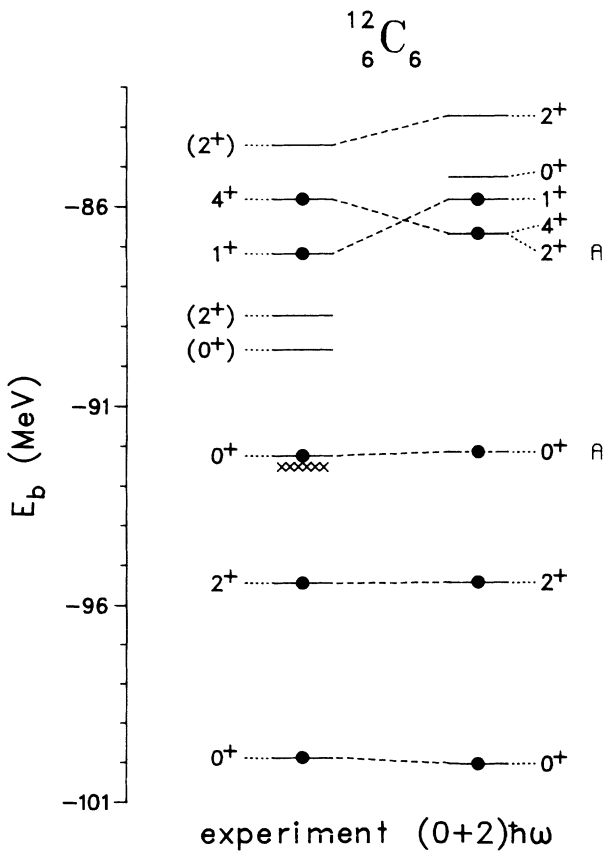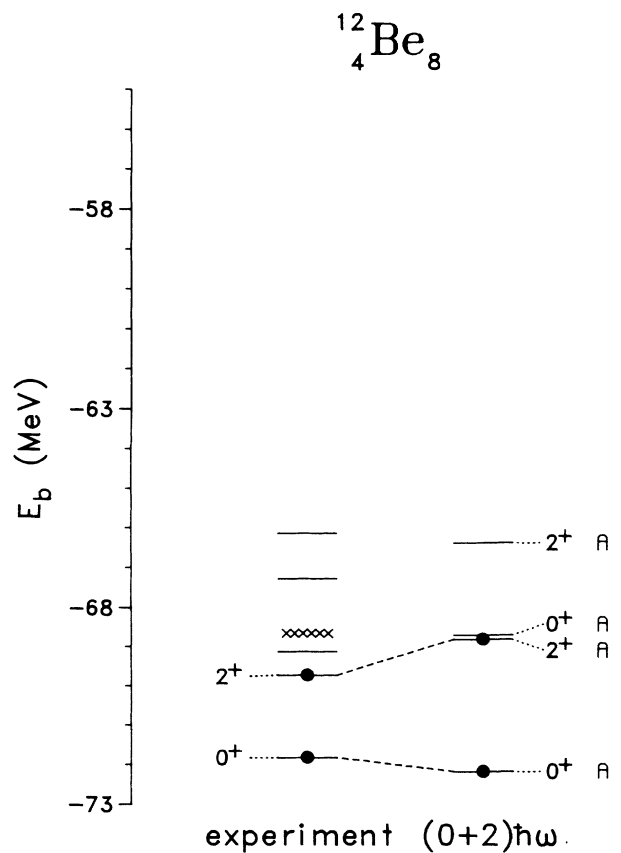
FIG. 21. Spectrum of ^{14}N. See also caption of Fig. 1.

reproduced in the present calculation as in almost any $0\hbar\omega$ shell-model calculation. All other states included in the fit are intruder states. For nearly all calculated states one finds a good to fair agreement with experimental data, including the 5^+ state, which has the highest spin observed so far. The theoretical 1_4^+ state should be identified as a radial excitation. Although this state is expected near the particle breakup threshold, it might have a significant width such that it has escaped experimental detection. The calculated 1_5^+ state would then agree very well with one of the experimental 1^+ states at $E_b \approx -105$ MeV.

^{14}C: The agreement with experiment for the calculated energies of the intruder states 0_2^+, 2_2^+, 0_3^+, and 4_1^+ in ^{14}C is very good; see Fig. 22. The experimental level with $J \geq 1$ might correspond with the calculated 2_4^+ state. At $E_x = 14.7$ MeV (not shown) a high-spin state is observed experimentally with a tentative assignment $J^\pi = 6^+$ or 5^-. The present result for the 6^+ yrast state yields $E_x = 16.3$ MeV.

L. Mass $A = 15$ nuclei

^{15}N: The nucleus ^{15}N, as well as its mirror nucleus ^{15}O, is well investigated experimentally. One has obtained spin assignments for many low-lying normal-parity states, while moreover a large number of nonnormal-parity states, not discussed here, have been identified. Except for the yrast $\frac{1}{2}^-$ and $\frac{3}{2}^-$ states all levels in ^{15}N are intruder states. The obtained spectrum, see Fig. 23, agrees

in general very well with experiment. A problem seems the appearance of two $\frac{1}{2}^-$ states within 0.1 MeV in the calculation at about $E_b = -117.6$ MeV ($E_x = 8.4$ MeV), since there is no experimental indication for a second $\frac{1}{2}^-$ state in this region of excitation energy so far. The highest spin observed for a normal-parity state is $\frac{11}{2}$ and it is well reproduced here.

^{15}C: All normal-parity states in ^{13}C are, according to our definition, intruders. It follows from Fig. 24 that good agreement between experiment and theory exists. Above $E_b = -109$ MeV we calculate several states with high spin, which are not observed experimentally. The calculated $\frac{5}{2}^-$, $\frac{7}{2}^-$, and $\frac{9}{2}^-$ states at $E_x \approx 6.0$ MeV might correspond with three experimental states at $E_x \approx 6.4$ MeV tentatively assigned $(\frac{5}{2}, \frac{7}{2}^+, \frac{9}{2}^+)$, $(\frac{3}{2}, \frac{5}{2}, \frac{7}{2})$, and $(\frac{9}{2}^-, \frac{11}{2})$, respectively. Strictly speaking we have calculated the $T = \frac{3}{2}$ states in ^{15}N, since in ^{15}C one neutron already occupies the sd shell and thus cannot be excited into the sdg shell in our space.

M. Mass $A = 16$ nuclei

^{16}O: At the upper end of the p shell nearly all levels become intruder states. In ^{16}O only the ground state can be obtained in a $0\hbar\omega$ model space; see Fig. 25. The second 0^+ state, which is calculated about 1 MeV too high is found to be predominantly a state with $[f] = [4444]$ and SU(3) quantum numbers $(\lambda\mu) = (20)$. This is in conflict
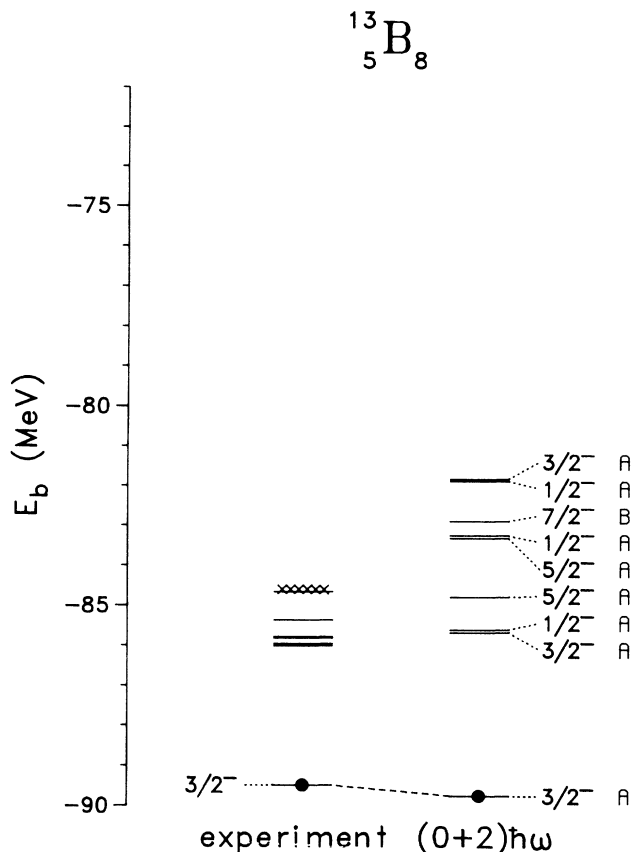

FIG. 22. Spectrum of ^{14}C. See also caption of Fig. 1.
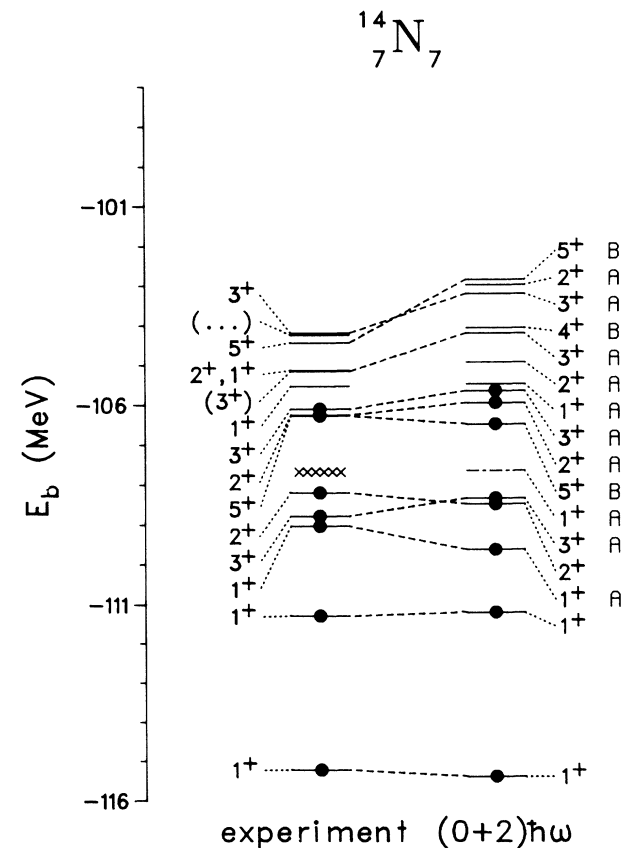

FIG. 23. Spectrum of ^{15}N. See also caption of Fig. 1.

with the recent calculations of Hayes *et al.*,[16] that predict the 0_2^+ to be predominantly of $4\hbar\omega$ character with $(\lambda\mu)=(84)$. The latter classification also follows from the weak-coupling model in which one assumes the 0_2^+ state to be of 4p-4h character.[17] The present calculation gives quite reasonable values for the $E0$ matrix elements, however; see Sec. VI.

^{16}N: The spectrum of ^{16}N, presented in Fig. 26, shows a rather high-level density. The 2^- ground state cannot be taken into account in the present description. There is good agreement with experiment for most of the excited states. An exception is the theoretical 0^+ level, which is not reported in the compilations of experimental $T=1$ levels in $A=16$ nuclei. In fact we calculated the $T=1$ states in ^{16}O for the same reason as explained for ^{15}C.

III. THE STRUCTURE OF THE WAVE FUNCTIONS

The subject of this section is the structure of the wave functions that are obtained with the present interaction.

A. Ground states

Figure 27 shows the structure of the resulting wave functions of the $A=4-16$ ground states with $T=0$ or $T=\frac{1}{2}$ in the (0+2)$\hbar\omega$ model space. The five different components are labeled as follows:

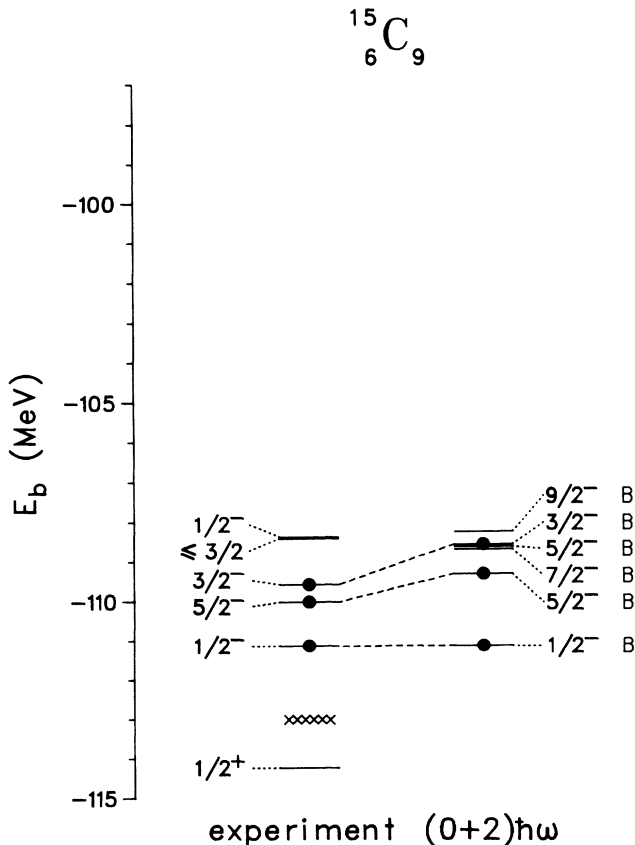(I) $p^2\rightarrow(sd)^2$ stands for $(0s)^4(0p)^{A-6}(1s0d)^2$, possible for $A\geq6$ only.

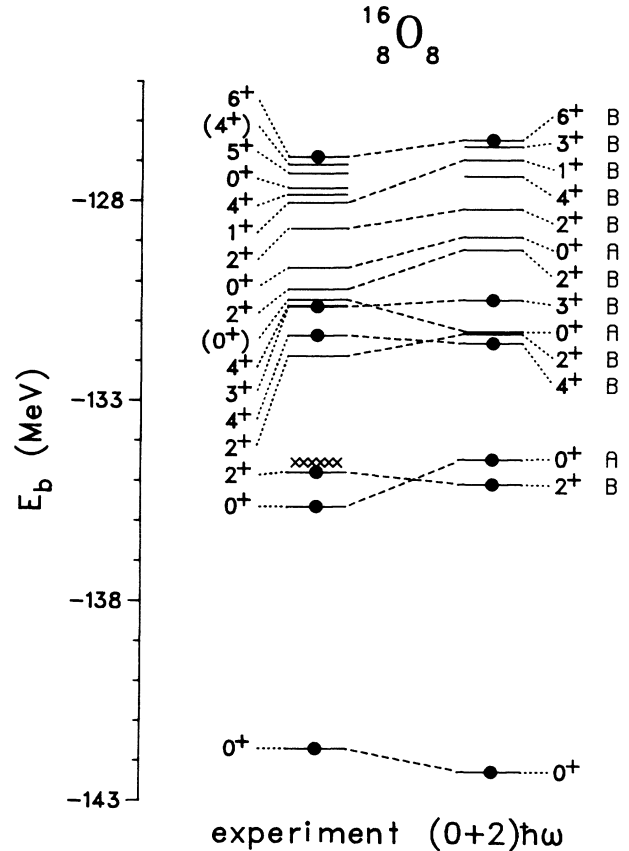FIG. 25. Spectrum of ^{16}O. See also caption of Fig. 1.

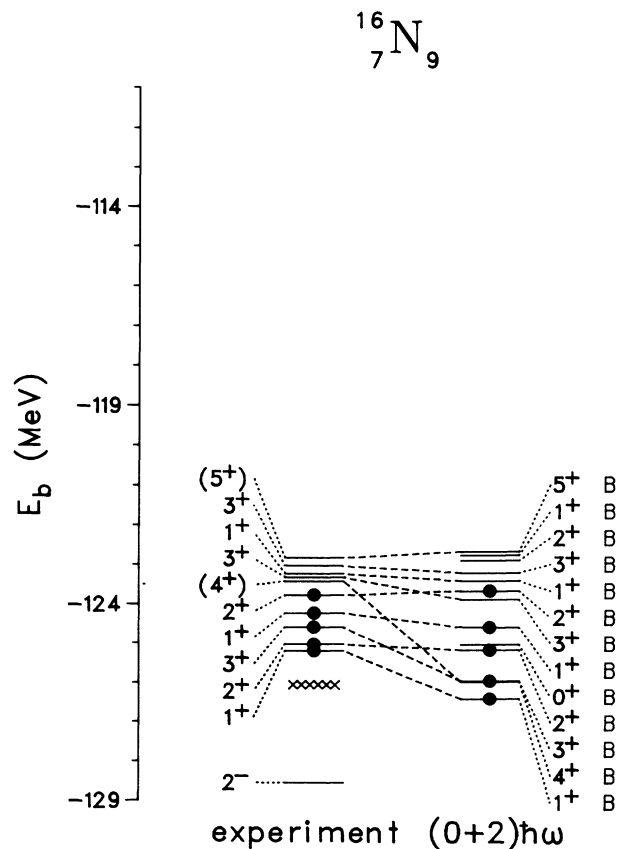FIG. 24. Spectrum of ^{15}C. See also caption of Fig. 1.

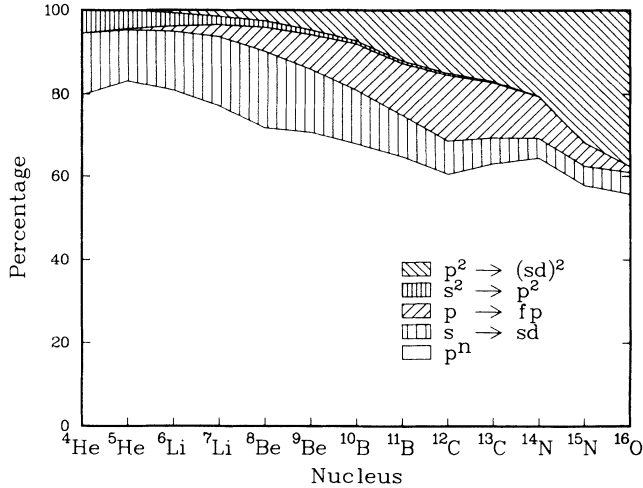FIG. 26. Spectrum of ^{16}N. See also caption of Fig. 1.

FIG. 27. Structure of the ground-state wave functions of the $A = 4{-}16$ nuclei with $T = 0$ or $T = \frac{1}{2}$, obtained with the present interaction. For the notation, see text.

(II) $s^2 \rightarrow p^2$ stands for $(0s)^2(0p)^{A-2}$, possible for $A \leq 14$ only.

(III) $p \rightarrow fp$ stands for $(0s)^4(0p)^{A-5}(0f1p)^1$, possible for $A \geq 5$ only.

(IV) $s \rightarrow sd$ stands for $(0s)^3(0p)^{A-4}(1s0d)^1$.

(V) p^n stands for $(0s)^4(0p)^{A-4}$.

It follows from Fig. 27 that the most important contribution to the structure of these waves functions is, as expected, the $0\hbar\omega$ component $(0s)^4(0p)^{A-4}$. This component varies from 80% for ^{4}He to 56% for ^{16}O. As a consequence the total intensity of the $2\hbar\omega$ components increases quite strongly from 20% for ^{4}He to 44% for ^{16}O. The $2\hbar\omega$ components can be divided into two classes: the one-particle, one-hole (1p-1h) excitations ($s \rightarrow sd$ and $p \rightarrow fp$) and the two-particle, two-hole (2p-2h) excitations [$s^2 \rightarrow p^2$ and $p^2 \rightarrow (sd)^2$]. It follows from Fig. 27 that the character of the ground states changes considerably with respect to these classes. In the very light nuclei ($A \leq 9$) the 1p-1h excitations are mainly responsible for the $2\hbar\omega$ intensities. For the wave functions of the nuclei in the middle of the p shell ($10 \leq A \leq 14$) we see a mixture of both classes, where the 2p-2h excitations become more important for larger A-values. Finally for the $A \geq 15$ nuclei the $2\hbar\omega$ components are dominated by the 2p-2h excitations. Of the 44% $2\hbar\omega$ components in ^{16}O as much as 38% consist of 2p-2h excitations.

Looking at each type of component separately one sees from Fig. 27 that the $p^2 \rightarrow (sd)^2$ component increases strongly with an increasing A. The other 2p-2h contribution, $s^2 \rightarrow p^2$, is decreasing when the mass increases from $A = 4$ to $A = 16$. This is obvious, because for increasing A the p shell fills up with nucleons, leaving less vacancy for nucleons excited from the s shell. The $p \rightarrow fp$ component increases until a maximum of 16% in ^{12}C and then strongly drops to 1.5% in ^{16}O. The intensity of the other 1p-1h excitation, $s \rightarrow sd$, is roughly a factor two to three larger in the $A = 4{-}10$ nuclei than in the heavier $A = 13{-}16$ nuclei.

B. Intruder states

To discuss the structure of the intruder states, we present in Table I the intensities of the five types of components which contribute to the wave functions. The notation for these components has been explained above. We will restrict ourselves only to low-lying 0^+, 2^+, and 4^+ intruder states in several nuclei. To demonstrate the differences between these intruder states and the predominant $0\hbar\omega$ levels, also the structure of several levels of the latter are added in Table I. Furthermore it is indicated in Table I whether an intruder state belongs to class A or class B; see Sec. II.

The first observation is the fact that all class A intruder states contain a relatively small amount, less than 20%, of $0\hbar\omega$ components. By definition, see Sec. I, the class B intruder states cannot contain $0\hbar\omega$ components. Further we see that for the three 0^+ intruders in $A = 4$, $A = 10$, and $A = 12$ the structure is mainly determined by the 1p-1h excitations, while for the 0^+ states in heavier nuclei the 2p-2h contributions dominate the structure completely. This is the same situation as for the ground states: for heavier nuclei 2p-2h components are dominant, while in the lighter nuclei the 1p-1h contributions are most important.

Remarkable is the fact that the class-B states in Table I have a very simple structure, almost 100% $p^2 \rightarrow (sd)^2$. Hence these states contain only a very small percentage of 1p-1h components; this in contrast to most class-A intruders, where the 1p-1h structure is much more important.

IV. CHARGE rms RADII

The first observable we study is the charge rms radius. With the assumption that one uses harmonic-oscillator wave functions, it can be shown[13] that the charge radius within a $0\hbar\omega$ model space is independent of the structure of the wave function and only depends on the value of the harmonic-oscillator size parameter b.

In a $(0+2)\hbar\omega$ model space the latter property does not hold anymore. In this case the charge radius not only depends on b, but also on the structure of the wave functions. This is due to the fact that matrix elements $\langle nl|r^2|n\pm1l \rangle$ contribute to the rms radius for a mixed $(0+2)\hbar\omega$ wave function, but not for a pure $0\hbar\omega$ wave function. Due to interference effects the rms charge radius, expressed in units of b, may be smaller in the $(0+2)\hbar\omega$ space than in the $0\hbar\omega$ space.

There are several ways to determine the value of the size parameter b. The most consistent value might be the one derived from the presently obtained value for the parameter $\hbar\omega$ and the proton mass. However, when one applies[2] this value of b, denoted as $b_{\hbar\omega}$, to calculate the charge radii, one finds $b_{\hbar\omega} = 2.05$ fm. The resulting radii then become too large, a result obtained earlier in other calculations.[13,18]

Therefore we will use the effective value b_{rad}, which follows from a least-squares fit of calculated charge radii to the experimentally known values with the proton finite-size correction taken into account. We found, for the present wave functions in the $(0+2)\hbar\omega$ model space,

TABLE I. Components of the wave function (in %) for several 0^+, 2^+, and 4^+ states. For notation see text of Sec. III.

Nucleus	J^π	Class	$p^2 \to (sd)^2$	$s^2 \to p^2$	$p \to fp$	$s \to sd$	p^n
^{4}He	0_1^+	$0\hbar\omega$		5.5		14.7	79.8
	0_2^+	A		21.0		60.0	19.0
^{6}He	0_1^+	$0\hbar\omega$	0.5	2.9	0.2	13.5	82.9
	0_2^+	A	9.7	0.6	49.1	29.9	10.7
	2_1^+	$0\hbar\omega$	2.9	0.2	2.3	12.4	82.2
	2_2^+	$0\hbar\omega$	2.8	2.2	14.6	12.6	67.8
^{8}Be	0_1^+	$0\hbar\omega$	2.6	1.5	5.6	18.5	71.8
	0_2^+	A	7.3	0.4	45.5	43.8	3.0
	0_3^+	$0\hbar\omega$	8.0	1.0	16.2	18.4	56.4
	2_1^+	$0\hbar\omega$	2.1	1.3	6.1	19.6	70.9
	2_2^+	A	5.1	0.8	32.1	36.7	25.3
	2_3^+	$0\hbar\omega$	3.8	1.2	16.3	24.1	54.6
	4_1^+	$0\hbar\omega$	1.0	0.8	7.9	21.6	68.7
	4_2^+	A	3.4	0.8	23.7	36.8	35.3
^{10}Be	0_1^+	$0\hbar\omega$	8.4	0.8	8.7	12.4	69.7
	0_2^+	A	13.5	0.1	55.2	28.0	3.2
	2_1^+	$0\hbar\omega$	8.2	0.6	8.1	13.7	69.4
	2_2^+	$0\hbar\omega$	8.5	0.6	8.6	14.2	68.1
^{12}C	0_1^+	$0\hbar\omega$	14.9	0.5	16.0	8.1	60.5
	0_2^+	A	13.5		42.5	25.5	18.5
	2_1^+	$0\hbar\omega$	15.5	0.4	8.9	9.5	65.7
	4_1^+	$0\hbar\omega$	15.2		7.5	11.7	65.6
^{14}C	0_1^+	$0\hbar\omega$	32.4	0.1	8.6	5.1	53.8
	0_2^+	A	86.3		3.2	0.9	9.6
	2_1^+	A	38.1		7.4	6.6	47.9
	2_2^+	A	91.4		2.0	0.9	5.7
	4_1^+	B	99.4		0.6		
^{16}O	0_1^+	$0\hbar\omega$	37.6		1.5	5.2	55.7
	0_2^+	A	80.5		16.3	3.1	0.1
	2_1^+	B	99.1		0.9		
	2_2^+	B	95.9		3.8	0.3	
	4_1^+	B	99.4		0.6		
	4_2^+	B	98.5		1.5		

the value $b_{\mathrm{rad}} = 1.75$ fm. This is significantly smaller than $b_{\hbar\omega}$. In the $0\hbar\omega$ model space we found $b_{\mathrm{rad}} = 1.71$ fm.

In Fig. 28 the calculated and experimental charge rms radii of several ground states of p-shell nuclei are shown. The reported experimental values are obtained from de Vries *et al.*[19] From Fig. 28 it follows that both the $0\hbar\omega$ and the $(0+2)\hbar\omega$ calculation reproduce the general increase of the radii with increasing mass number A. Compared to the results in a $0\hbar\omega$ model space, the radii of ^{4}He and ^{16}O can be better reproduced in the larger $(0+2)\hbar\omega$ model space. As a result of $2\hbar\omega$ admixtures the radius of ^{4}He decreases, whereas that of ^{16}O increases. However, looking more precisely, one observes that the details cannot be obtained in the present calculation under the assumption that b is mass independent. In particular the relatively large experimental radius of ^{6}Li cannot be explained in either model space.

V. STATIC MOMENTS

We have explained that static moments have been included in the fitting procedure to determine the effective
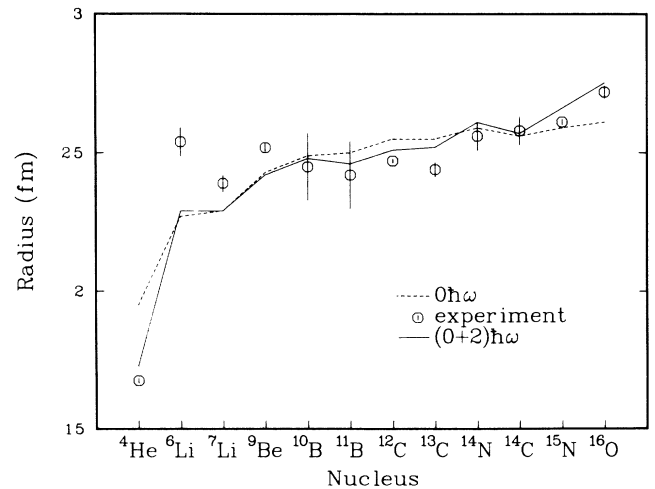

FIG. 28. The charge rms radius of several ground states in $0\hbar\omega$ and $(0+2)\hbar\omega$ model spaces compared to the experimental values. In the $0\hbar\omega$ space $b = 1.71$ fm, while in the $(0+2)\hbar\omega$ space $b = 1.75$ fm.

interaction; see paper I. The empirical strength parameters for the $\mathcal{M}1$ and $\mathcal{E}2$-operators are determined simultaneously.

For a derivation of the expressions for the required electromagnetic operators the reader is referred to Brussaard et al.,[20] in which also the applied long-wavelength approximation is explained. Furthermore center-of-mass recoil corrections, leading to some A and Z dependence of the strength parameters for these operators, will be ignored. These corrections are small.[20]

A. Magnetic dipole moments

The effective $\mathcal{M}1$ operator we use is completely characterized by the values of four parameters, i.e., the spin and the orbital g factors of a proton and a neutron.

In Table II the resulting effective nucleon spin and orbital g factors for various interactions are given together with the corresponding values for the bare protons and neutrons, which have been taken from Chaloupka et al.[21] The g factors for the (8–16)POT interaction[14] are obtained by fitting the dipole moments to the experimental data, while keeping the wave functions fixed. Furthermore the calculation of van Hees et al.[13] included dipole moments of $1\hbar\omega$ states too, which of course could not be reproduced in the two other calculations. The presented rms deviations $\Delta\mu_{\text{rms}}$ are based on one and the same set of dipole moments of predominantly $0\hbar\omega$ states.

From Table II it follows that the magnetic dipole moments in the current calculation yields the smallest deviation $\Delta\mu_{\text{rms}}$, in particular compared to the (8–16)POT results. However, the effective nucleon g-factors deviate somewhat more from the bare-nucleon values. This holds in particular for the orbital isovector part $g_l^{T=1}=g_l^p-g_l^n=1.32$, which deviates more than 30% from the bare-nucleon value, while the spin isovector part and the orbital and spin isoscalar parts are within 10% of the corresponding bare-nucleon values. In a recent investigation on p-shell nuclei in a $(0+2)\hbar\omega$ model space[22] it is shown that the inclusion of meson-exchange currents reduces the need for such large effective g-factors, in particular for the isovector part.

Table III shows all presently known magnetic dipole moments of normal-parity states in the p-shell nuclei, together with the values obtained in the present calculation. The experimental values can be found in Ajzenberg.[4–7] From Table III it follows that the presently obtained magnetic dipole moments deviate at most $0.10\mu_N$ from their experimental values.

TABLE III. Magnetic dipole moments (μ_N).

Nucleus	J^π	Experiment[a]	Theory
^{6}Li	1^+	0.822	0.835
^{7}Li	$\frac{3}{2}^-$	3.256	3.302
^{8}Li	2^+	1.653	1.576
^{8}B	2^+	1.036	1.072
^{9}Li	$\frac{3}{2}^-$	3.439	3.460
^{9}Be	$\frac{3}{2}^-$	−1.178	−1.172
^{10}B	3^+	1.801	1.845
	1^+	0.63±0.12	0.672
^{11}B	$\frac{3}{2}^-$	2.689	2.754
^{11}C	$\frac{3}{2}^-$	−0.964	−0.981
^{12}B	1^+	1.003	0.937
^{12}N	1^+	0.457	0.435
^{13}B	$\frac{3}{2}^-$	3.178	3.075
^{13}C	$\frac{1}{2}^-$	0.702	0.661
^{13}N	$\frac{1}{2}^-$	−0.322	−0.257
^{14}N	1^+	0.404	0.386
^{15}N	$\frac{1}{2}^-$	−0.283	−0.301
^{15}O	$\frac{1}{2}^-$	0.719	0.724

[a]Error, if not specified, less than one unit in the last digit.

B. Electric quadrupole moments

The matrix elements of $O(\mathcal{E}LM)$ between harmonic-oscillator states with a size parameter b are proportional to b^L. Therefore when the harmonic-oscillator size parameter b is not fixed, the strength parameters of an effective $\mathcal{E}2$ operator should be given in units $b^2 e_p$ and $b^2 e_n$ instead of just e_p and e_n. These values are optimized in the fitting procedure described in paper I. Table IV shows the obtained strength parameters of the $\mathcal{E}2$ operator together with the rms deviation for the quadrupole moments. As for the magnetic dipole moments, see Sec. V, we present results for three interactions. For the Cohen and Kurath (8–16)POT interaction we again kept the wave functions fixed and optimized $b^2 e_p$ and $b^2 e_n$ in a fit to quadrupole moments only.

Besides the significant reduction of ΔQ_{rms} compared to the other two calculations, the most important difference of the present calculation compared to previous calculations on light nuclei is the very small value for $b^2 e_n$; see Table IV. Using $b_{\text{rad}}=1.75$ fm, which followed from the optimalization of the charge radii, see Sec. IV, one finds $e_p=1.19e$ and $e_n=0.06e$.

One often assumes for the isovector part of the $\mathcal{E}2$ operator the relation $e_p-e_n=1e$. Writing $e_p=1e+\Delta e_p$ and $e_n=\Delta e_n$, one obtains $\Delta e_p=\Delta e_n$. From the currently

TABLE II. g factors and rms deviations for dipole moments.

	Bare nucleon value	(8–16)POT (Ref. 14)	$(0+1)\hbar\omega$ (Ref. 13)	Present results
g_l^p	1.000	1.058	1.030	1.183
g_l^n	0.000	−0.013	0.036	−0.136
g_s^p	5.586	5.510	5.543	5.906
g_s^n	−3.826	−3.821	−3.875	−4.174
$\Delta\mu_{\text{rms}}(\mu_N)$		0.123	0.050	0.047

TABLE IV. Strength parameters for the $\mathcal{E}2$ operator and rms deviations for quadrupole moments.

	Bare nucleon value	(8–16)POT (Ref. 14)	$(0+1)\hbar\omega$ (Ref. 13)	Present results
$b^2 e_p$	b^2	3.61	3.64	3.63
$b^2 e_n$	0	1.39	1.36	0.18
$\Delta Q_{\text{rms}}(e\ \text{fm}^2)$		0.50	0.34	0.23

obtained ratio $b^2 e_p / b^2 e_n = 20$, see Table IV, one thus finds $\Delta e = 0.05e$, which yields $e_p = 1.05e$ and $e_n = 0.05e$. This assumption, however, leads to a harmonic-oscillator size parameter $b = 1.86$ fm.

In this $(0+2)\hbar\omega$ calculation the matrix elements of the bare $\mathcal{E}2$ operator are in general much larger than in $0\hbar\omega$ calculations. As a result it is not necessary anymore to use large effective charges in order to reproduce the experimental quadrupole moments. The explanation of this phenomenon lies in the fact that in the present description the giant quadrupole resonance is included in the model space. Besides matrix elements which are diagonal in the number of oscillator quanta, the one-body $\mathcal{E}2$ operator has also nonvanishing matrix elements between two states if their number of oscillator quanta differs by 2. Hence the $\mathcal{E}2$ operator gives contributions of the type $0\hbar\omega \leftrightarrow 0\hbar\omega$, $2\hbar\omega \leftrightarrow 2\hbar\omega$, but also $0\hbar\omega \leftrightarrow 2\hbar\omega$. Especially the latter, which are of course absent in a $0\hbar\omega$ space, add in most cases coherently and thus lead to stronger $\mathcal{E}2$ strengths (and quadrupole moments). The $\mathcal{M}1$ operator gives only contributions which are diagonal in the number of quanta (in any harmonic oscillator shell-model space). Therefore the magnetic dipole moments are much less sensitive to changes in the model space than the quadrupole moments.

In Table V the values for the experimentally known quadrupole moments are presented and compared with the calculated values. The experimental data are taken from Ajzenberg.[4-7] We see a remarkably good agreement between theory and experiment, except for the sign of the very small quadrupole moment of ^{6}Li.

After the determination of the present effective interaction for which the experimental quadrupole moments listed in Table IV have been used, a new compilation on $A = 5-10$ nuclei appeared,[23] containing additional information on some experimental quadrupole moments. Three of these moments differ from the values presented in Table V. The new values are $Q(^6\text{Li}) = -0.08$ e fm^2, $Q(^7\text{Li}) = [-4.06\pm0.08]$ e fm^2 and $Q(^9\text{Li}) = [-3.6 \pm 0.6]$ e fm^2.

VI. TRANSITION STRENGTHS

Transition strengths give a good indication about the structure of wave functions. Therefore they form a good test case for the current interaction. Because only normal-parity states are involved, we consider $\mathcal{M}1$ and $\mathcal{E}2$ transition strengths.

A. $\mathcal{M}1$ transition strengths

In general one finds a good agreement between experiment and calculation.[2] Even the very small $\mathcal{M}1$ strengths are mostly reproduced as far as the order of magnitude is concerned.

B. $\mathcal{E}2$ transition strengths

We find a quite good agreement between experiment and calculation[2] for nuclei with $A \leq 13$. The theoretical values are obtained with the values $b^2 e_p = 3.63$ e fm^2 and $b^2 \cdot e_n = 0.18$ e fm^2, that follow from the fit of the quadrupole moments in the determination of the interaction.

Reasonable values could not be obtained for several of the $\mathcal{E}2$ transitions in the nuclei with $A \geq 14$. Despite the rather good reproduction of the spectra for these nuclei, one finds in particular for ^{16}O that the $(0+2)\hbar\omega$ model space is too restricted to explain some very strong transitions. For a correct description of these strengths we expect that the inclusion of $4\hbar\omega$ components in the wave functions is very important.

VII. Logft VALUES

Most of the allowed β decay takes place between states with predominantly a $0\hbar\omega$ character. There exists a reasonable agreement between theory and experiment.[2] The most serious problem seems to consist of the logft values for transitions between the 0^+ states in the mirror nuclei ^{14}C and ^{14}O, and the first 1^+ state in ^{14}N. The applied operator[20] leads to the same logft value for both transitions. The calculated transition strength is several orders of magnitudes larger than the experimental strengths, which show strong retardation.

VIII. FORM FACTORS

To describe electron scattering, form factors are indispensable. A form factor F can be separated into two parts F_L and F_T, the longitudinal and transverse form factor, respectively. These form factors contain all nuclear-structure information and are a function of the transferred momentum q. The longitudinal form factor F_L is a sum over coulomb form-factor components, denoted by $F_{C\lambda}$, while the transverse form factor F_T consists of a sum over electric and magnetic form-factor components, denoted by $F_{E\lambda}$ and $F_{M\lambda}$, respectively. The multipole order λ satisfies the relation

$$|J_i - J_f| \leq \lambda \leq J_i + J_f \tag{1}$$

with J_i and J_f the spin of the initial and final state, respectively. The form-factor components can be obtained by means of a multipole expansion of the fourier trans-

TABLE V. Electric quadrupole moments (e fm^2).

Nucleus	J^π	Experiment[a]	Theory
^{6}Li	1^+	-0.06 ± 0.01	0.08
^{7}Li	$\frac{3}{2}^-$	-3.70 ± 0.08	-3.50
^{8}Li	2^+	2.4 ± 0.2	2.62
^{9}Li	$\frac{3}{2}^-$	-3.3 ± 0.7	-3.55
^{9}Be	$\frac{3}{2}^-$	5.3 ± 0.3	4.87
^{10}B	3^+	8.47 ± 0.06	8.63
^{11}B	$\frac{3}{2}^-$	4.07 ± 0.03	4.42
^{11}C	$\frac{3}{2}^-$	3.43	3.26
^{12}B	1^+	1.34 ± 0.14	1.53
^{12}C	2^+	6 ± 3	6.50
^{13}B	$\frac{3}{2}^-$	4.78 ± 0.46	4.30
^{14}N	1^+	1.56	1.45

[a]See text for other values.

form of the transition matrix elements. These are the matrix elements of the nuclear charge and current-density operators. For a more detailed discussion of form factors we refer to other publications.[24,25]

Two corrections will be applied to the calculated form factors. The first one is a result of the center-of-mass motion that is included in any shell-model wave function of a nuclear state. For harmonic-oscillator radial wave functions it has been shown,[26] that this effect can be exactly compensated for. The correction[24] consists of the multiplication of any calculated shell-model form-factor component with a simple factor $f_{c.m.}(q)$

$$f_{c.m.}(q) = e^{q^2 b^2/4A} . \tag{2}$$

The second correction concerns the finite size of nucleons. Instead of assuming that nucleons are point particles, one has to multiply the obtained form factor by a single-nucleon form factor $F_{fs}(q)$ to correct for this effect. We use the two-pole form factor[27]

$$F_{fs}(q) = \left[1 + \frac{q^2}{(855 \text{ MeV})^2} \right]^{-2} . \tag{3}$$

This correction factor is an approximate expression for the single-nucleon form factor, i.e., the form factor that represents the internal structure of the nucleon. It is applied to all form-factor components. No corrections for meson exchange currents or relativistic effects are included.

In Figs. 29–31 we compare as typical examples some longitudinal and transverse form factors obtained from the $0\hbar\omega$[15] and the present $(0+2)\hbar\omega$ wave functions with experimental data. Form factors for several other states can be found in Wolters.[2] Bare-nucleon transition operators are used, i.e., the proton charge e_p and neutron charge e_n were fixed to $1e$ and $0e$, respectively. Besides the bare values for the proton and neutron dipole mo-
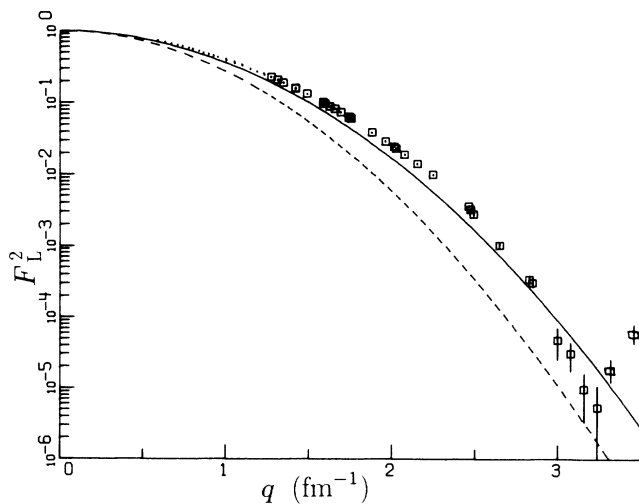
ments were applied, $\mu_p = 2.79\mu_N$ and $\mu_n = -1.91\mu_N$, respectively. To avoid the introduction of more parameters, as state-dependent b values, we use the harmonic-oscillator size parameters $b = 1.71$ fm and $b = 1.75$ fm for the $0\hbar\omega$ and $(0+2)\hbar\omega$ model spaces, respectively. These values are the same as those used for the calculation of ground-state charge radii; see Sec. IV. However, this choice is not necessarily optimal.

In the $0\hbar\omega$ model space the $C0$ form factors in all p-shell nuclei are independent of the wave function. The only freedom, apart from the finite-size correction, is the scaling along the q axis which is effected by varying the size parameter b. For ^{4}He the $0\hbar\omega$ form factor is given by

$$F(q) = e^{-b^2 q^2/4} F_{fs}(q) f_{c.m.}(q) , \tag{4}$$

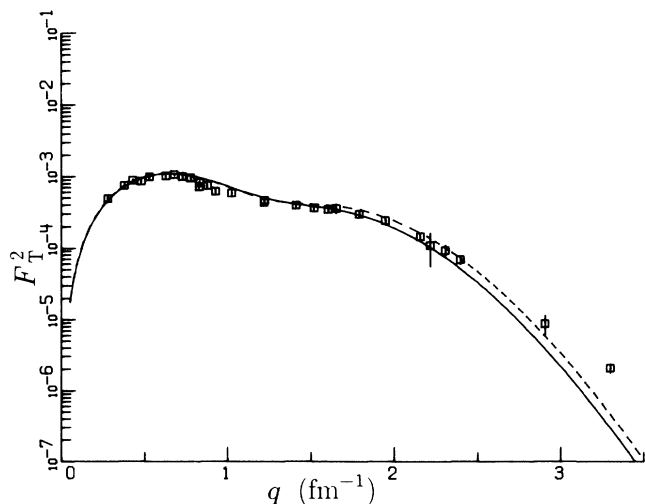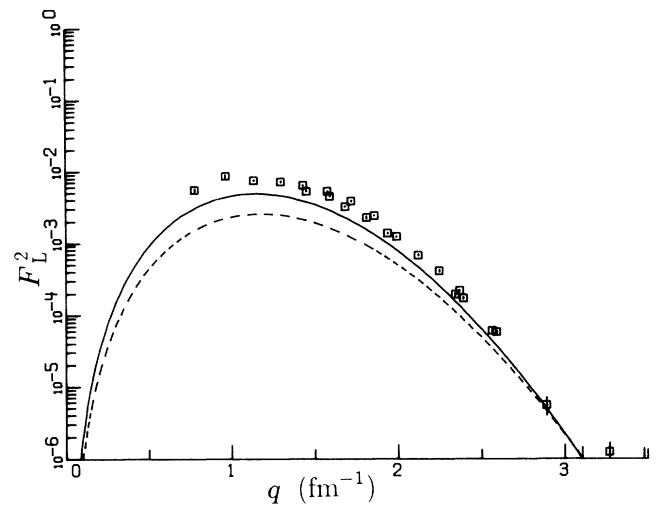where $F_{fs}(q)$ and $f_{c.m.}(q)$ are defined in (3) and (2), re-

FIG. 30. Longitudinal (top) and transverse (bottom) form factor for the first $J^\pi = \frac{1}{2}^-$; $T = \frac{1}{2}$ state of ^{7}Li. The points represent the experimental data (Refs. 30 and 31). See also caption of Fig. 29.

FIG. 29. Longitudinal form factor for elastic scattering on the $J^\pi = 0^+$, $T = 0$ ground state of ^{4}He. The solid line is obtained in the $(0+2)\hbar\omega$ space, while the dashed line shows the $0\hbar\omega$ result. The points represent the experimental data (Refs. 28 and 29).
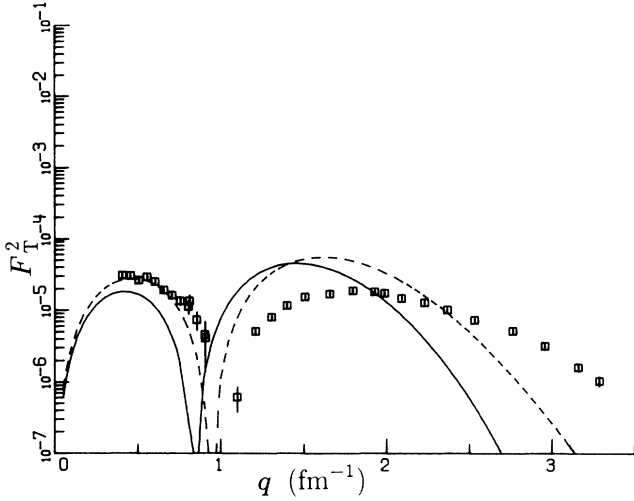
FIG. 31. Transverse form factor for elastic scattering on the $J^\pi = \frac{1}{2}^-$, $T = \frac{1}{2}$ ground state of ^{13}C. The points represent the experimental data. (Refs. 32 and 33). See also caption of Fig. 29.

spectively. The $2\hbar\omega$ admixtures in the ground-state wave function gives considerable additional freedom, leading to the form factor for the ^{4}He ground state that has the form[25]

$$F(q) = \left[1 + \alpha \left[\frac{bq}{2} \right]^2 + \beta \left[\frac{bq}{2} \right]^4 \right] e^{-b^2 q^2/4} F_{fs}(q) f_{\text{c.m.}}(q) \ ,$$

(5)

where α and β are determined by the structure of the wave functions. A sufficiently negative value of α would result in a node in the form factors. Since β is in general negligible, one finds the node at about

$$q = (-\alpha)^{-1/2} \frac{2}{b} \ .$$

(6)

Since the minimum is found experimentally at $q \approx 3$ fm^{-1}, see Fig. 29, and the value of b we used is 1.75 fm, we find that

$$\alpha = -\frac{4}{b^2 q^2} = -0.124 \ .$$

(7)

However, from our wave functions we deduce $\alpha = +0.213$, i.e., there is no node. On the other hand the current positive value of α leads to a significant decrease of the charge rms radius, which improves agreement with experiment; see Sec. IV.

The general behavior of the various form factors for ground states and excited states is reproduced to some extent in both the $0\hbar\omega$ and $(0+2)\hbar\omega$ model space. For instance the form factor for the first $\frac{1}{2}^-$ state in ^{7}Li is reproduced quite well; see Fig. 30. Serious discrepancies between theory and experiment occur, however, in the transverse form factors $F_T(q)$ for the $J^\pi = \frac{1}{2}^-$ ground state of ^{13}C; see Fig. 31.

With the present assumptions about effective charges,

nucleon g factors and b values the differences between the $0\hbar\omega$ and $(0+2)\hbar\omega$ results are generally less than a factor of two for the regions where $F(q)$ does not vary too strongly with q. Larger deviations between the two sets of wave functions are found in the high-q region. An extension of the model space from $0\hbar\omega$ to $(0+2)\hbar\omega$, which is shown to be quite successful for energies, static moments and transition rates, does not considerably improve the calculated form factors.

It may thus be concluded that the present deviations between experimental and theoretical form factors probably stem from an effective interaction that is not optimal, a still too small model space, or should possibly be attributed to relativistic effects or mesonic degrees of freedom which are not taken into account in the present description.

IX. CONCLUSIONS

The conclusions from the present approach to correlate a large number of observables in $A = 4-16$ nuclei with a mass-independent phenomenological interaction are summarized in the following points.

(1) Properties of many intruder states can be reproduced correctly.

(2) The $2\hbar\omega$ admixtures are substantial. For the ground states they increase from 20% for ^{4}He to 44% for ^{16}O.

(3) The description of predominant $0\hbar\omega$ states is often improved considerably. This holds in particular for electric quadrupole moments and $\mathscr{E}2$-transition strengths. Only very small effective charges are required to reproduce the experimental values of these observables.

(4) The description of nuclei at the lower and upper end of the p shell should be further improved by the inclusion of $N\hbar\omega$ components with $N \geq 4$. This holds in particular for ^{16}O.

(5) The discrepancies between theory and experiment for form factors are not solved by the inclusion of the $2\hbar\omega$ components. Possibly the current model space is still too small or relativistic and/or mesonic effects play a significant role.

For a similar description of nonnormal-parity states one needs to include $1\hbar\omega$ and $3\hbar\omega$ components in the wave functions. Therefore to reproduce both normal-and nonnormal-parity states in the same space, the model space must be expanded to a $(0+1+2+3)\hbar\omega$ space. This should be feasible with present-day computer facilities.

Much more information about results of the present calculations can be found in Wolters,[2] which is available upon request.

[1]A. A. Wolters, A. G. M. van Hees, and P. W. M. Glaudemans, Phys. Rev. C **42**, 2053 (1990), the preceding paper.

[2]A. A. Wolters, Ph.D. thesis, Utrecht University, 1989.

[3]S. Fiarman and W. E. Meyerhof, Nucl. Phys. **A206**, 1 (1973).

[4]F. Ajzenberg-Selove, Nucl. Phys. **A413**, 1 (1984).

[5]F. Ajzenberg-Selove, Nucl. Phys. **A433**, 1 (1985).

[6]F. Ajzenberg-Selove, Nucl. Phys. **A449**, 1 (1986).

[7]F. Ajzenberg-Selove, Nucl. Phys. **A460**, 1 (1986).

[8]G. M. Hale and D. C. Dodder, in *Proceedings of the Tenth International Conference on Few Body Problems in Physics,* edited by B. Zeitnitz (North-Holland, Amsterdam, 1984), Vol. II, p. 433.

[9]R. Ceuleneer, P. Vandepeutte, and C. Semay, Phys. Lett. B **196**, 303 (1987).

[10]R. Ceuleneer, P. Vandepeutte, and C. Semay, Phys. Rev. C **38**, 2335 (1988).

[11]J. P. Elliott, A. D. Jackson, H. A. Mavromatis, E. A. Sanderson, and B. Singh, Nucl. Phys. **A121**, 241 (1968).

[12]J. J. Bevelacqua, Phys. Rev. C **33**, 699 (1986).

[13]A. G. M. van Hees and P. W. M. Glaudemans, Z. Phys. A **314**, 343 (1983); **315**, 223 (1984).

[14]S. Cohen and D. Kurath, Nucl. Phys. **73**, 1 (1965).

[15]A. G. M. van Hees, A. A. Wolters, and P. W. M. Glaudemans, Phys. Lett. B **196**, 19 (1987); Nucl. Phys. **A476**, 61 (1988).

[16]A. C. Hayes, J. L. Friar, and D. Strottman, Phys. Rev. C **41**, 1727 (1990).

[17]A. Arima, H. Horiuchi, and T. Sebe, Phys. Lett. B **24**, 129 (1967).

[18]A. A. Wolters, A. G. M. van Hees, and P. W. M. Glaudemans, Europhys. Lett. **5**, 7 (1988).

[19]H. de Vries, C. W. de Jager, and C. de Vries, At. Data Nucl. Data Tables **36**, 495 (1987).

[20]P. J. Brussaard and P. W. M. Glaudemans, *Shell-Model Applications in Nuclear Spectroscopy* (North-Holland, Amsterdam, 1977).

[21]V. Chaloupka, C. Bricman, A. Barbado-Galtieri, D. M. Chew, R. L. Kelly, T. A. Lasinski, A. Rittenberg, A. H. Rosenfeld, T. G. Trippe, F. Uchimaya, N. Barash-Schmidt, P. Söding, and M. Roos, Phys. Lett. **50B**, 1 (1974).

[22]J. G. L. Booten, A. G. M. van Hees, and P. W. M. Glaudemans, Phys. Rev. C (to be published).

[23]F. Ajzenberg-Selove, Nucl. Phys. **A490**, 1 (1988).

[24]T. deForest, Jr. and J. D. Walecka, Adv. Phys. **15**, 1 (1966).

[25]H. Überall, *Electron Scattering from Complex Nuclei* (Academic, New York, 1971).

[26]L. J. Tassie and F. C. Barker, Phys. Rev. **111**, 940 (1958).

[27]T. M. Donnelly and I. Sick, Rev. Mod. Phys. **56**, 461 (1984).

[28]J. J. McCarthy, I. Sick, and R. R. Whitney, Phys. Rev. C **15**, 1396 (1977).

[29]R. F. Frosch, J. S. McCarthy, R. E. Rand, and M. R. Yearian, Phys. Rev. **160**, 874 (1967).

[30]G. J. C. van Niftrik, L. Lapikás, H. de Vries, and G. Box, Nucl. Phys. **A174**, 173 (1971).

[31]J. Lichtenstadt, J. Alster, M. A. Moinester, J. Dubach, R. S. Hicks, G. A. Peterson, and S. Kowalski, Phys. Lett. B **219**, 394 (1989).

[32]L. Lapikás, G. Box, and H. de Vries, Nucl. Phys. **A253**, 324 (1975).

[33]R. S. Hicks, J. Dubach, R. A. Lindgren, B. Parker, and G. A. Peterson, Phys. Rev. C **26**, 339 (1982).